University of Glasgow | Experimental Particle Physics

GLAS-PPE/2009-27
8th December 2009

Department of Physics and Astronomy
Experimental Particle Physics Group
Kelvin Building, University of Glasgow,
Glasgow, G12 8QQ, Scotland
Telephone: +44 (0)141 330 2000 Fax: +44 (0)141 330 5881

LHCb Collaboration LHCb 2009-004

A non-parametric method to estimate the Forward Backward Asymmetry from the $B_d \to K^* \mu^+ \mu^-$ decay at LHCb

F Marinho[a,*], C Parkes[a], S Viret[a,b]

[*] *Corresponding author*

[a] The University of Glasgow, Dept. of Physics and Astronomy, Glasgow, G12 8QQ.

[b] Now at CNRS, Clermont-Ferrand

Abstract

This note discusses the use of a non-parametric unbinned method to evaluate the dimuon mass squared distribution and the Forward Backward asymmetry (FBA) from the $B_d \to K^* \mu^+ \mu^-$ decay. This method gives access to the complete shape of the FBA distribution: the FBA zero point is obtained directly, no straight line fit or other assumptions on the shape of the distribution are required. The implementation of this approach and the results obtained using simulated events are presented. The sensitivity obtained for the FBA zero point was $\sigma_{ZeroPoint} = 0.40 \pm 0.04$ GeV$^2/c^4$ for an integrated luminosity of 2 fb^{-1}.

1 Introduction

This note presents a non-parametric unbinned method to evaluate the dimuon mass squared distributions and Forward-Backward asymmetry (FBA) of the $B_d \to K^*\mu^+\mu^-$ rare decay at LHCb. The method is based on a Kernel approach which does not assume any a priori model or parametrisation of the distributions obtained.

This note considers only the estimation of the FBA. However, the method is general and can be applied to other relevant observables in this decay or to the full angular analysis. A binned fit implementation of the full angular analysis for LHCb can be found in [1]. A companion note discusses the implementation of acceptance corrections and background subtraction in this approach (see [2]).

This note is organised as follows. Section 2 provides an overview of the theoretical background related to the $B_d \to K^*\mu^+\mu^-$ rare decay, describing some of the quantities which will be measured in LHCb. Section 3 presents the unbinned method implementation and the results obtained for the FBA calculations. A final discussion about the method and its results is given in section 4.

2 Theoretical Introduction

The $B_d \to K^*\mu^+\mu^-$ decay is a flavour changing neutral current process (FCNC) which occurs only via loop diagrams. This decay has been measured at Babar and Belle and its branching ratio was found to be $1.10^{+0.29}_{-0.26} \times 10^{-6}$ [3]. This is compatible with the branching ratio of $1.19 \pm 0.39 \times 10^{-6}$ estimated with next-to-next leading order calculations in the Standard Model (SM) [4]. Figure 1 shows two of the lowest order Feynman diagrams of the $B_d \to K^*\mu^+\mu^-$ decay. A number of quantities can be measured for this decay such as the dimuon mass distribution, forward-backward asymmetry and information obtained on the Wilson coefficients (see [5] for a recent review). Analyses have been performed at Babar and Belle and the results are in agreement with the SM. However, the uncertainties are still large due to the statistics available and more precise measurements are necessary.

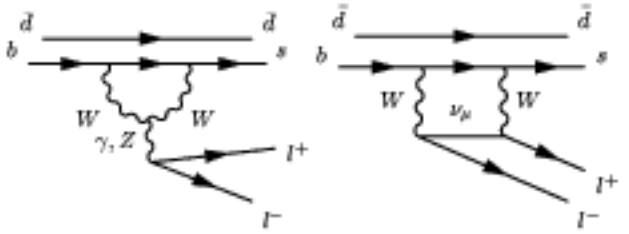

Figure 1: Box and Penguin diagrams for $B_d \to K^*\mu^+\mu^-$.

In many extensions of the SM the differential branching ratio and the angular distributions can drastically change [6, 7]. Measurements of the $B_d \to K^*\mu^+\mu^-$ decay at LHCb will allow searches for new physics effects (NP). Figure 2 shows examples of additional Feynman diagrams due to NP models with new particles inside the loop. These kinds of contribution can potentially affect the angular distributions of the $B_d \to K^*\mu^+\mu^-$ decay.

2.1 Observables in $B_d \to K^*\mu^+\mu^-$ analysis

A number of quantities that can provide good estimates to confirm the SM predictions or to spot NP have been identified in many theory papers (see [4, 6, 7, 8, 9, 10]). This section describes those quantities that are also interesting from an experimental point of view, as they are relatively easy to measure. All formulas and quantities shown in this section were calculated in [11, 12].

It is convenient to express the differential spectrum in terms of an angular decomposition. This decomposition provides direct access to measurable quantities of interest [12]. The double-differential

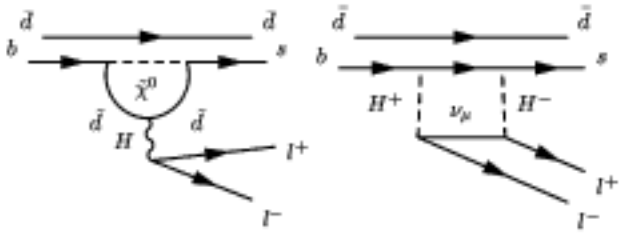

Figure 2: Examples of SUSY Feynman diagrams for $B_d \to K^* \mu^+ \mu^-$. A penguin diagram with a virtual Neutralino and squarks is shown on the left-hand side. A box diagram with charged Higgs bosons is shown on the right-hand side.

spectrum formula is given by,

$$\frac{d^2\Gamma}{dq^2 dcos\theta_l} = \frac{3}{8}\left[(1+cos^2\theta_l)H_T(q^2) + 2cos\theta_l H_A(q^2) + 2(sin^2\theta_l)H_L(q^2)\right], \tag{1}$$

where q is the dimuon invariant mass and θ_l is the angle between l^+ and the B meson calculated in the dimuon rest frame. The H_X functions can be written as quadratic combinations of transversity amplitudes. These amplitudes are given in terms of the Wilson coefficients and hadronic form factors. The Wilson coefficients describe the perturbative part of the Hamiltonian and the hadronic form factors are functions which contain all the information from the non-perturbative part of the Hamiltonian.

From the double differential branching ratio it is possible to derive quantities such as the dimuon mass spectrum and the forward backward distribution to obtain information on the Wilson coefficients.

The differential branching ratio as a function of the dimuon mass is obtained by simply integrating over the angle θ_l in equation 1,

$$\frac{d^2\Gamma}{dq^2} = H_T(q^2) + H_L(q^2). \tag{2}$$

Figure 3 shows the squared dimuon mass distribution calculated in the SM and also in some Supersymmetry models [7]. The SM, SUGRA and MIA-SUSY models are shown. The shaded area illustrates the typical hadronic uncertainties. The peaks are due to the $c\bar{c}$ resonances. The two main peaks are due to the J/Ψ and $\psi\prime$ resonances.

A theoretically cleaner measurement that can be made with the $B_d \to K^* \mu^+ \mu^-$ decays is the so-called Forward Backward Asymmetry (FBA). The FBA can be interpreted as the difference between the number of forward-events and the number of backward-events as a function of the dimuon mass squared. An event is classified as forward if $\theta_l \leq \pi/2$ and backward if $\theta_l > \pi/2$. This quantity provides a powerful measurement to test the SM and to search for NP. This curve has a particular shape that could change significantly as NP enters the Hamiltonian.

The FBA is defined as,

$$\mathcal{A}_{FB}(q^2) = \int_{-1}^{1} \frac{d^2\Gamma}{dq^2 dcos\theta_l} sgn(cos\theta_l) dcos\theta_l, \tag{3}$$

and by substituting the expression given at equation 1 it is possible to write the FBA as,

$$\mathcal{A}_{FB}(q^2) = \frac{3}{4} H_A(q^2). \tag{4}$$

Not only the shape of the FBA distribution is important but also the point where its value is zero. This point is commonly referred to as the FBA zero point. The FBA zero point provides the ratio between the coefficients C_7 and C_9 with the theoretical uncertainties reduced to a minimum. This measurement is important because both C_7 and C_9 Wilson coefficients are susceptible to NP contributions and a considerable shift on their expected values would be an indication of NP.

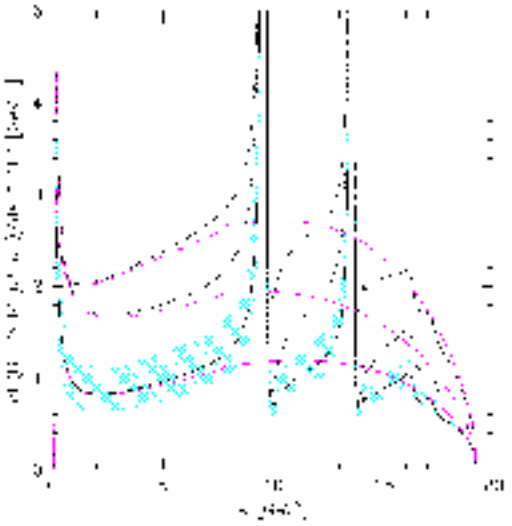

Figure 3: Squared dimuon mass distribution for SM and various SUSY models. The solid line represents the SM. The dashed line represents a SUGRA model and long-short dashed line represents a MIA-SUSY model. The purple lines correspond to the pure short-distance spectra. Figure reproduced from [7].

Figure 4 shows the FBA calculated in the SM. Results using different values for the Wilson coefficients are shown. The values in table 1 have been used to make the three extra curves in the graph.

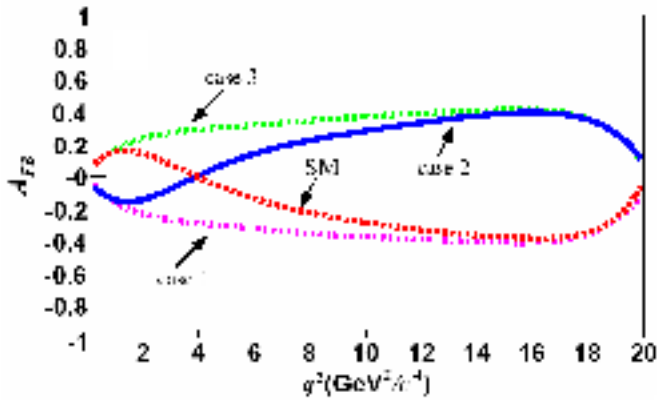

Figure 4: Forward backward asymmetry distribution calculated in the SM. Each case assumes different values for the Wilson coefficients (see table 1). Figure reproduced from [13].

3 The Forward Backward Asymmetry in LHCb

As defined in section 2.1, the FBA is the difference between the number of forward-events and backward-events as a function of the dimuon mass squared. In previous analyses the FBA dependence with the dimuon mass squared was obtained by dividing the dimuon mass squared range in to bins. This approach was used in the Babar and Belle analyses [13, 14], and also in the previous studies in LHCb described in [15, 16]. In this section an alternative approach to measure the FBA is described. This novel technique uses a non-parametric unbinned method to estimate the FBA distribution.

Table 1: Different values of Wilson coefficients used for FBA calculations.

case 1	$C_7 = -C_7^{SM}, C_9 = C_9^{SM}, C_{10} = C_{10}^{SM}$
case 2	$C_7 = C_7^{SM}, C_9 C_{10} = -C_9^{SM} C_{10}^{SM}$
case 3	$C_7 = -C_7^{SM}, C_9 C_{10} = -C_9^{SM} C_{10}^{SM}$

This method gives access to the complete shape of the FBA distribution. No straight line fit, or other assumptions on the shape of the distribution, are required to obtain the FBA zero point.

This unbinned method provides full access to the distribution's shape. Unlike the binned method, the value of the distribution can be calculated at any position without fitting or interpolating. The unbinned method converges to the true distribution with a smaller (or at worst the same) number of events as the unbinned method. As a consequence of these features the FBA zero point calculation needs no further model-dependent fit or parametrisation. In the previous LHCb analyses the FBA zero point was obtained by fitting polynomials to a binned distribution. The determination of the zero point provided by these fits depends on the dimuon mass squared range used in the fit and on the order of the polynomial (typically a straight line fit). Instead in this non-parametric method the zero point can be found directly.

Section 3.1 describes the simplified Monte-Carlo (MC) simulation used to develop the unbinned method. Section 3.2 explains the implementation of the unbinned method and how it is used to calculate the FBA. The estimates obtained for the FBA and its uncertainties are presented. The concept of the Kernel density estimator is introduced and the convergence properties of the method considered. A method to estimate the smoothness parameter, which play a similar role to the bin size in a histogram method, is discussed.

3.1 Simplified Monte Carlo

A simplified MC simulation was used to develop the unbinned method and to calculate the uncertainties on the estimates provided. In this simplified model no detector simulation was included. This reduced the simulation time drastically and allowed this toy MC to generate the number of events necessary to perform the analysis proposed in a short period of time[4)].

The results from [15, 16, 17] indicated that the dimuon mass and the θ_l angle are determined to a high precision in LHCb. Therefore, no significant distortions on the shape of the generator level distribution of these variables are expected after the LHCb event reconstruction. This also indicates that the results obtained with this toy MC should not differ significantly from what would be expected with the complete LHCb simulation.

In this analysis 100 data sets were generated. Each set contained the number of signal events equivalent to the estimated annual LHCb yield of ~ 7k events [16, 17] . Each of these data sets were then analysed, using the method described in section 3.2. The FBA and its zero point were estimated, and the LHCb sensitivity to measure the FBA was evaluated using all the data sets.

The LHCb simulation software was used to generate the events [18]. The detector response was not emulated, only geometrical requirements were applied to ensure the particles produced in the $B_d \to K^* \mu^+ \mu^-$ decay were inside the detector acceptance. No selection cuts on the particles were introduced at this level.

3.2 Unbinned Method

This section describes the unbinned method developed to obtain the FBA distribution in the $B_d \to K^* \mu^+ \mu^-$ analysis. To calculate the FBA it was necessary: to evaluate which events were forward or

[4)] The time necessary to generate a single event with the complete LHCb simulation is $\sim 70\,s$.

backward; to obtain the dimuon mass squared distribution for the forward and backward events; and to use the obtained distributions to evaluate the FBA according to equation 5.

The FBA distribution is given by:

$$\mathrm{FBA}(\mathrm{M}^2_{\mu^+\mu^-}) = \frac{\mathrm{Forward}(\mathrm{M}^2_{\mu^+\mu^-}) - \mathrm{Backward}(\mathrm{M}^2_{\mu^+\mu^-})}{\mathrm{Forward}(\mathrm{M}^2_{\mu^+\mu^-}) + \mathrm{Backward}(\mathrm{M}^2_{\mu^+\mu^-})}, \tag{5}$$

where Forward (Backward) is the differential number of forward (backward) events.

The following sections describe the nonparametric unbinned method developed to measure the FBA. Section 3.2.1 introduces the unbinned method and its features. Section 3.2.2 discusses the convergence of the method when applied to the dimuon mass and FBA distributions. Sections 3.2.3 and 3.2.4 explain how the unbinned method was used to analyse the 2 fb^{-1} simulated data sets and presents the results obtained.

3.2.1 Kernel Density Estimator

In this section a method to evaluate the probability density functions (pdf) is introduced. This approach is a nonparametric unbinned method which does not assume a specific shape for the distribution. Such methods are useful in cases where the distribution is unknown or difficult to parametrise with a reduced number of parameters.

This method estimates the pdf by relacing each of the observed data points with a Gaussian or other function (denoted K below) and summing up these contributions. The width of the K function used to represent each point controls the smoothness of the distribution and is denoted h below.

In general, the pdf can be obtained by using a sequence of independent and identically distributed random events. Given a data set represented as $x_1,\ x_2,\ x_3,\ ..., x_n$ distributed according to $f(x)$ one can estimate the pdf as:

$$f_n(x) = \frac{1}{nh}\sum_{i=1}^{n} K\left(\frac{x_i - x}{h}\right), \tag{6}$$

where K are the kernel functions defined as

$$K(y) \geq 0, \quad K(y) = K(-y),$$
$$\lim_{|y|\to\infty} yK(y) = 0, \quad \int_{-\infty}^{\infty} K(y)dy = 1,$$

and h is the smoothness parameter[6]. Theoretical background on the convergence of this kind of estimator and further generalisations related to relaxed conditions of continuity can be found in [19, 20, 21]. In this analysis a Gaussian function was used as the kernel K.

The best choice for the value of h depends on the total number of events used to calculate the pdfs and on the shape of the distribution itself. To obtain sensible results the value for the h parameter used must be within an acceptable range, $h_{min} < h < h_{max}$. This range of suitable h values becomes broader as the number of events used for the pdfs calculation increases. If h is outside this range two problems can occur: overfit and underfit. Overfit means that statistical fluctuations are reproduced as true features of the pdf ($h < h_{min}$). Underfit ($h > h_{max}$) results in the loss of information in the calculation of the distribution. Figure 5 illustrates the overfit and underfit effects. The method used to evaluate the appropriate h value for this analysis is discussed in section 3.2.3.

Note that the role of the h parameter is similar to the bin width when using histograms. Overfit and underfit also occur with histograms if the bin width is not appropriate. With histograms the bin width can be reduced as the number of events increases. The bin width choice is also constrained

[6] The formula given by equation 6 can be referred to as the expression of the Kernel Density Estimator. It is also called the Parzen Estimator, after Emanuel Parzen who developed this method in [19].

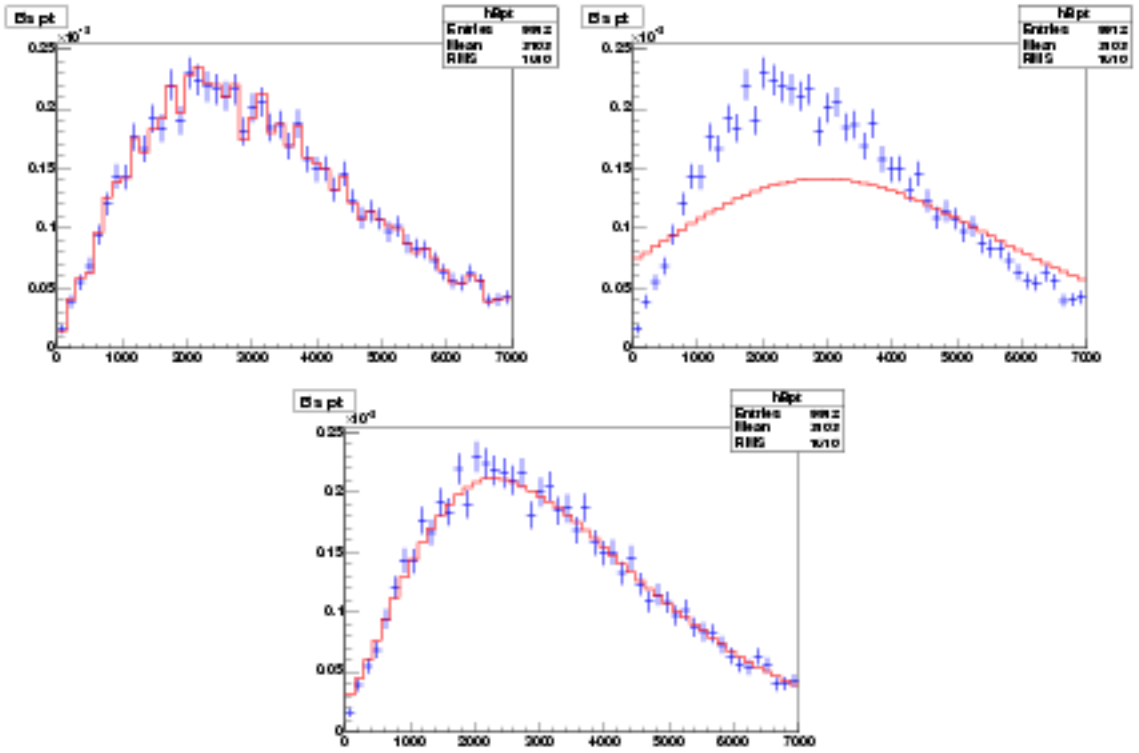

Figure 5: Comparison between kernel density estimator and histogram. The red lines are the values calculated with the kernel density estimator and the blue markers represent a binned histogram estimate of the same distribution. On the top row overfit and underfit examples are shown. On the left-hand side an example of the overfit effect is shown. On the right-hand side the underfit effect is shown. The bottom row figure shows the pdf estimate using an appropriate h. Extracted from [22].

by the shape of the distribution, as is the h parameter: the bins used to describe sharp peaks are in general smaller than those used in the distribution's tails.

However, in a binned distribution the bins are typically all the same size, while the h parameter is in general defined as a function of x. Hence, it can depend on the shape of the distribution. In regions of the distribution with narrow peaks or steep gradients the appropriate h values to use are smaller than those that should be used in the distribution's tails.

3.2.2 Method Convergence

A set of ~ 700k events was used to evaluate the dimuon mass and FBA distributions with the unbinned method. Using such large statistics allowed the pdf estimate to be h independent. The results were then compared with estimates obtained with histograms in order to verify the convergence of the method.

Figure 6 shows the comparison between the dimuon mass squared distributions calculated with the unbinned method and by using histograms. In the case of high statistics the distributions converge to the same result.

The FBA distribution was evaluated by using the obtained dimuon mass distributions in the formula given by equation 5. The FBA formula was then written as

$$FBA(M^2_{\mu^+\mu^-}) = \frac{N_{forward} f_{forward}(M^2_{\mu^+\mu^-}) - N_{backward} f_{backward}(M^2_{\mu^+\mu^-})}{N_{forward} f_{forward}(M^2_{\mu^+\mu^-}) + N_{backward} f_{backward}(M^2_{\mu^+\mu^-})}, \tag{7}$$

where $N_{forward}$ ($N_{backward}$) was the total number of forward (backward) events selected and $f_{forward}$ ($f_{backward}$) was the dimuon mass squared distribution of the forward (backward) events.

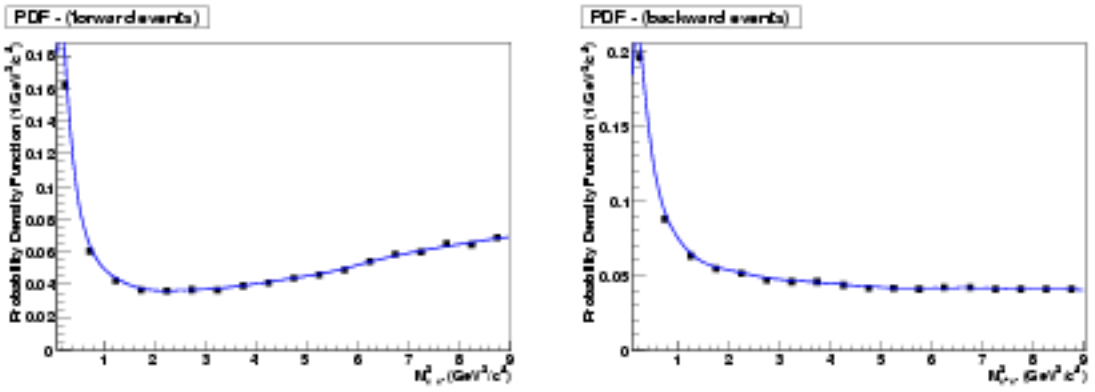

Figure 6: Dimuon mass squared distribution. Comparison between the unbinned estimate and the coarse histogram in the case of very high statistics. The curved line shows the unbinned method estimate and the black squares indicate the binned histogram estimates. On the left-hand side the distributions for the forward events are shown. On the right-hand side the distributions for the backward events are shown.

Figure 7 shows the comparison between the FBA distribution obtained with the unbinned method and with a coarse binned histograms for high statistics. The unbinned method and the histogram method provided similar estimates for the FBA. However the unbinned method provided access to the complete shape of the FBA distribution and the zero point could be extracted directly from the curve obtained. In the binned method the FBA zero point is typically extracted by fitting a straight line through a number of points in this region. Hence, the binned method assumes a straight line shape, which could be affected by NP. This assumption is not required in the unbinned method, but rather the point at which the distribution crosses the axis can be calculated directly.

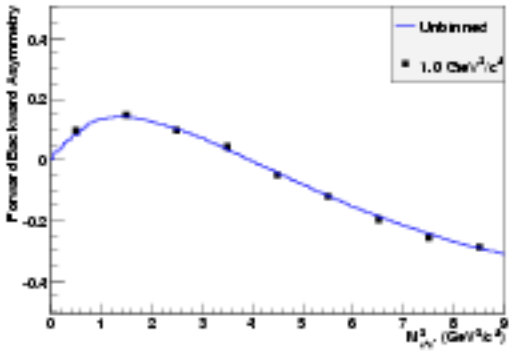

Figure 7: FBA distribution. Comparison between unbinned and coarse histogram estimates. The curved line shows the unbinned method estimate. The black squares indicate the binned histogram estimates with $1\,\mathrm{GeV}^2/c^4$ intervals.

3.2.3 h Estimate

To evaluate the FBA with an amount of data equivalent to $2\ \mathrm{fb}^{-1}$ it was necessary to estimate the appropriate h value to be used. This section discusses the procedures used to estimate the h parameter as a function of the dimuon mass squared.

The h parameter was estimated through a χ^2 approach. The calculated pdf obtained with the unbinned method and the pdf obtained by counting events within a coarse bin were compared at a

given dimuon mass squared. From this comparison, a χ^2 was evaluated as a function of h. A range of acceptable h values was then obtained from the χ^2 distribution.

Binned and Unbinned Estimates

The pdf value $\left\langle f\left(M^2_{\mu^+\mu^-}\right)\right\rangle$ is estimated from the binned analysis by counting events within a coarse bin centred at the dimuon mass squared $M^2_{\mu^+\mu^-}$. It is defined by,

$$\left\langle f\left(M^2_{\mu^+\mu^-}\right)\right\rangle = \frac{n_{events}}{n_{Total}\,\Delta M}, \tag{8}$$

where n_{events} is the number of events within the coarse bin, n_{Total} is the total number of events in the sample and ΔM is the width of the coarse bin. The width of the coarse bin should not be too small, causing large statistical fluctuations, or too large, leading to over smoothing of the distribution. For the comparison presented here a value of $\Delta M = 1.25\ \mathrm{GeV^2/c^4}$ was used.

The pdf value $f\left(h, M^2_{\mu^+\mu^-}\right)$ can also be estimated for the unbinned method. The unbinned estimate is a function of the h smoothness parameter, which we are trying to optimise. For the comparison with the binned method, the unbinned method can be estimated at any dimuon mass squared ${M^2_{\mu^+\mu^-}}^j$ in the range of the coarse bin used by the binned method,

$$(M^2_{\mu^+\mu^-} - \Delta M/2) < {M^2_{\mu^+\mu^-}}^j < (M^2_{\mu^+\mu^-} + \Delta M/2). \tag{9}$$

and we choose to evaluate this at N points in the range of the bin. Hence the dimuon mass squared values used in the unbinned method are:

$${M^2_{\mu^+\mu^-}}^j = M^2_{\mu^+\mu^-} - \Delta M\left(\frac{1}{2} - \frac{j}{N}\right) \tag{10}$$

where j runs from 1 to N. N should be sufficiently large that the value of the distribution does not change significantly between neighbouring points. Here a value of 15 was used for N.

χ^2 Evaluation

For each of the N points in the coarse dimuon mass squared bin a χ^2 can be evaluated between the binned and unbinned methods, these values can then be averaged to produce an overall χ^2. Hence,

$$\chi^2\left(h, M^2_{\mu^+\mu^-}\right) = \sum_{j=1}^{N} \frac{1}{N-1}\left(\frac{f\left(h, {M^2_{\mu^+\mu^-}}^j\right) - \left\langle f\left(M^2_{\mu^+\mu^-}\right)\right\rangle}{\sigma}\right)^2, \tag{11}$$

where $\left\langle f\left(M^2_{\mu^+\mu^-}\right)\right\rangle$ is the binned pdf estimate, $f\left(h, {M^2_{\mu^+\mu^-}}^j\right)$ are the N unbinned estimates and σ is the uncertainty on $\left\langle f\left(M^2_{\mu^+\mu^-}\right)\right\rangle$.

Example χ^2 curves obtained from this procedure as a function of the smoothness parameter h are shown in figure 8. These graphs were obtained with one data set equivalent to $2\ \mathrm{fb}^{-1}$.

The h_{min} and h_{max} values were determined as the points where $(\chi^2 = 0.3)$. This value of 0.3 for the maximum χ^2 was chosen empirically to avoid underfit and overfit.

Optimal h Value

The optimal value of h could then be taken from the minimum of the χ^2 curve. However, as the distributions are asymmetric it is preferable to use a more central value of h. Hence, a weighted average of the h values in the range h_{min} and h_{max} was used. The weight w was taken as the value of the likelihood that can be obtained from the χ^2, $w = e^{-\chi^2}$. The value taken for the h parameter was

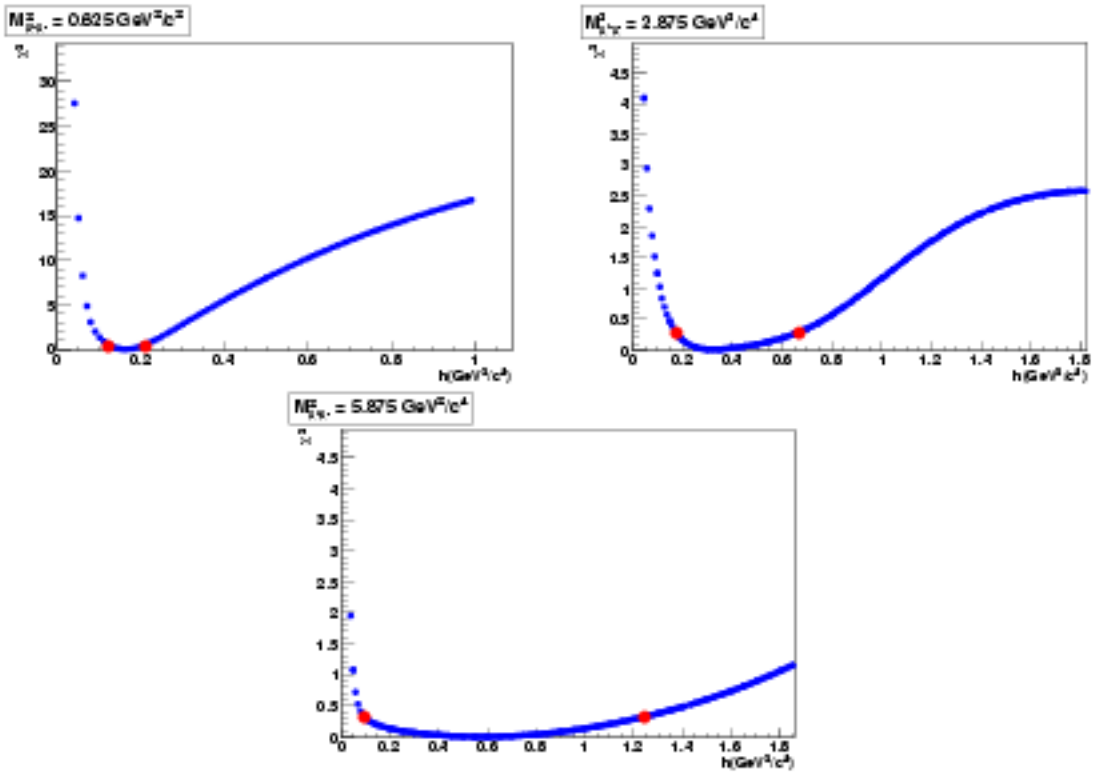

Figure 8: h optimisation. χ^2 distribution as a function of the h parameter at three different values of $M^2_{\mu^+\mu^-}$. The red dots show the points where $(\chi^2 = 0.3)$, which are used to determine the h_{min} and h_{max} values. These graphs were obtained with one data set equivalent to 2 fb^{-1}.

calculated as,

$$h = \frac{\int_{h_{min}}^{h_{max}} hw(h)dh}{\int_{h_{min}}^{h_{max}} w(h)dh}. \tag{12}$$

The h parameter was obtained as a function of the the dimuon mass squared by repeating this procedure for different values of $M^2_{\mu^+\mu^-}$. Figure 9 shows h as a function of $M^2_{\mu^+\mu^-}$. The values obtained for h did not vary significantly along the $M^2_{\mu^+\mu^-}$ axis. However, somewhat smaller values of h should be adopted at the lower $M^2_{\mu^+\mu^-}$ since the pdf distribution is steeply rising in that region with a pole at zero. In the example distribution shown in Figure 9, a straight line fit would be sufficient to obtain the h values. However, some distributions showed a greater curvature and hence a 3$^{\text{rd}}$ order polynomial was fitted to the distribution of h as a function of $M^2_{\mu^+\mu^-}$. The h functions obtained by this procedure were used to evaluate the FBA distribution in the following sections.

3.2.4 FBA Estimate

In this section the results obtained for the FBA using 2 fb^{-1} simulated data sets are presented. The h functions for the forward and backward events as discussed in section 3.2.3 were used to evaluate the dimuon mass distributions. The FBA was estimated by using the dimuon distributions together with equation 7.

Figure 10 shows the FBA obtained with four simulated data sets each equivalent to 2 fb^{-1}. The curves are compared with the expected FBA distribution calculated using 700k events as described in section 3.2.2.

The uncertainties shown in figure 10 were calculated by using the simplified MC. For each 2 fb^{-1} data set, the obtained dimuon mass distributions were used to sample about 100 new data sets with the same number of events. The FBA distribution was then evaluated for each of these new data sets and

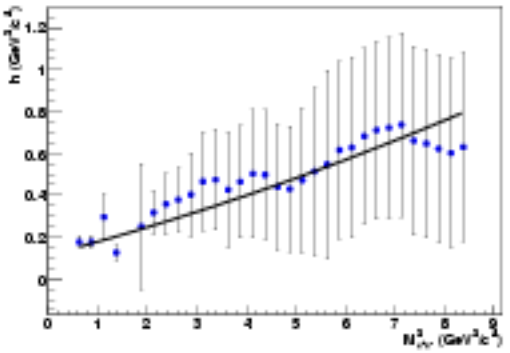

Figure 9: h as a function of $M^2_{\mu^+\mu^-}$. The blue dots indicate the optimal values of h calculated with equation 12. The errors indicate the $[\mathrm{h_{min}}, \mathrm{h_{max}}]$ range. The solid line is a fit performed with a 3^{rd} order polynomial.

the uncertainties were calculated as the RMS of each point of the curve. The quoted errors correspond to a $2\ \mathrm{fb}^{-1}$ data sample. Alternatively, an estimate of the uncertainty from a single data sample could be extracted using the jackknife method [23].

The data sets from the toy MC simulation were also used to calculate the FBA zero point sensitivity. Figure 11 shows the distribution of the values obtained for the zero point with all the data sets, i.e. split into $2\ \mathrm{fb}^{-1}$ data sets. The value obtained for the zero point was obtained through a Gaussian fit. The sigma from this fit is the estimate of the LHCb sensitivity to the measurement of the zero point. The zero point was estimated to be $\mathrm{S_0} = 3.95 \pm 0.05\ \mathrm{GeV^2/c^4}$ with a sigma of $\sigma_{\mathrm{S_0}} = 0.40 \pm 0.04\ \mathrm{GeV^2/c^4}$. This is in good agreement with the value and sensitivity obtained from the binned method [16].

4 Conclusions

A non-parametric unbinned method has been developed to evaluate the FBA distribution. The unbinned method provided access to the dimuon mass squared distributions and to the FBA distribution as continuous curves. A toy Monte Carlo simulation was used to evaluate the LHCb sensitivity to measure the FBA distribution. The FBA zero point sensitivity obtained was $\sigma_{\mathrm{S_0}} = 0.40\ \mathrm{GeV^2/c^4}$ for a integrated luminosity of $2\ \mathrm{fb}^{-1}$. An independent, similar, analysis has recently been performed [24] yielding consistent results with simlar sensitivity for S_0.

The results quoted here do not include reconstruction, selection and background effects. These effects are discussed in a companion note [2], where the possible sources of acceptance effects and how mismeasurement of the background distributions can affect the FBA distribution are presented.

References

[1] William Reece. Extracting Angular Correlations from the Rare Decay $\bar{B}_d \to \bar{K}^* \mu^+ \mu^-$ at LHCb. (CERN-LHCb-08-021).

[2] F. Marinho et al. Acceptance effects correction and background subtraction on the non-parametric method used in the Forward Backward Asymmetry calculation from the $B_d \to K^* \mu^+ \mu^-$ decay at LHCb. (CERN-LHCb-09-005).

[3] W.-M. Yao et al. 2006 Review of Particle Physics. *Journal of Physics G*, 33(1), 2006.

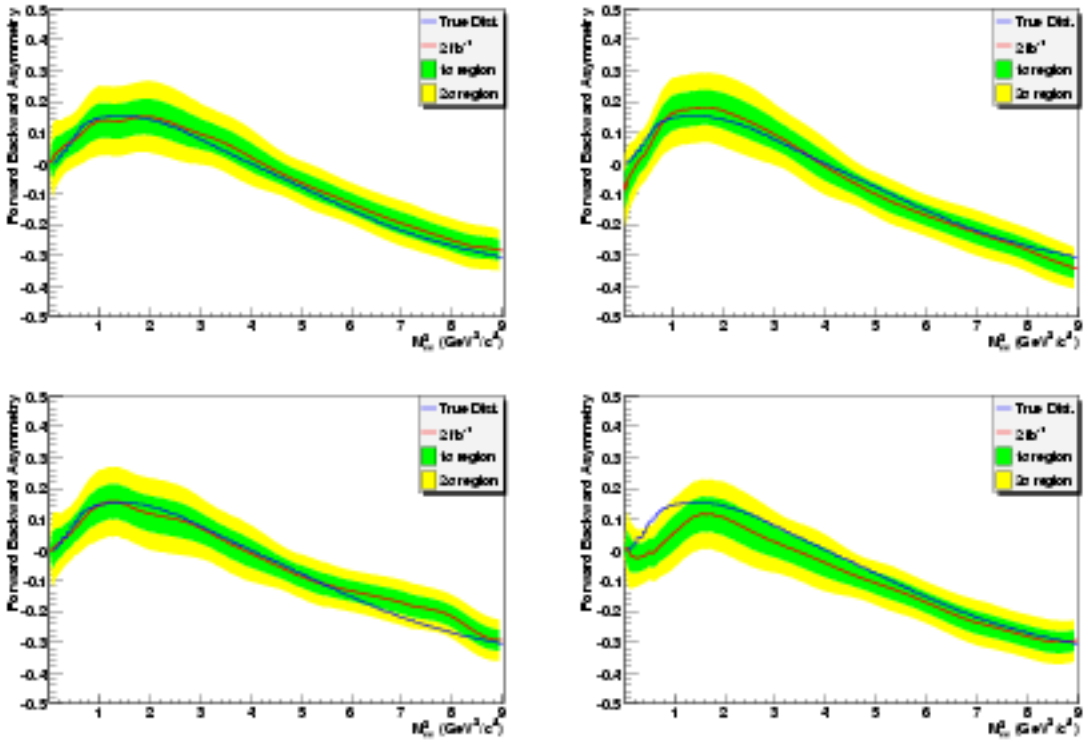

Figure 10: FBA obtained with 2 fb^{-1} data sets. Each graph was produced with a single data set. The red line represents the FBA calculated with a 2 fb^{-1} simulated data sample. The green and yellow areas represent 1σ and 2σ areas. The blue line represents the FBA as obtained in section 3.2.2, with large statistics.

[4] A. Ali, E.Lunghi, C. Greub, and G.Hillet. Improved model-independent analysis of semileptonic and radiative rare B decays. *Phys. Rev. D*, 66(034002), 2002.

[5] W. Altmannshofer et al. Symmetries and asymmetries of $B \to K^* \mu^+ \mu^-$ Decays in the Standard Model and Beyond. *JHEP*, 019(0901), 2009.

[6] M. Beneke, T. Feldmann, and D. Seidel. Systematic approach to exclusive $B \to V l^+ l^-, V\gamma$. *Nucl. Phys. B*, 612:25–58, 2001.

[7] A.Ali, P. Ball, L. T. Handoko, and G. Hiller. Comparative study of the decays $B \to K, K^* l^+ l^-$ in the Standard Model and supersymmetric theories. *Phys. Rev. D*, 61(074024), 2000.

[8] J. L. Hewett and J. D. Wells. Searching for Supersymmetry in rare B decays. *Phys. Rev. D*, 55:5549, 1997.

[9] E. Lunghi, A. Masiero, I. Scimemi, and L. Silvestrini. $B \to X_s l^+ l^-$ decays in Supersymmetry. *Nucl. Phys. B*, 568:120, 2000.

[10] G. Buchalla, G. Hiller, and G. Isidori. Phenomenology of non-standard Z^0 couplings in inclusive semileptonic $b \to s$ transitions. *Phys. Rev. D*, 63:014015, 2001.

[11] C. Bobeth, P. Gambino, M. Gorbahn, and U. Haisch. Complete NNLO QCD Analysis of $B \to X_s l^+ l^-$ and Higher Order Electroweak Effects. *JHEP*, 0404:71, 2004.

[12] K. S. M. Lee, Z. Ligeti, I. W. Stewart, and F. J. Tackmann. Extracting short distance information from $b \to s l^+ l^-$. *Phys. Rev. D*, 75:034016, 2007.

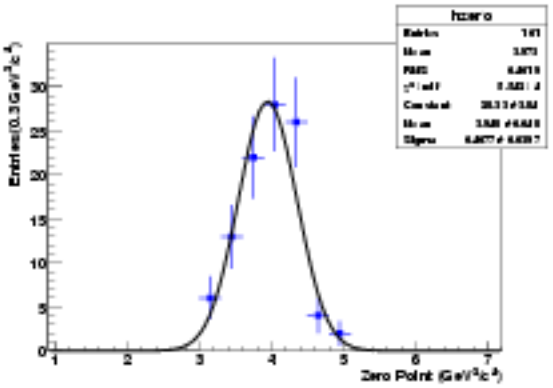

Figure 11: FBA zero point distribution. The FBA was estimated from 100 data samples each corresponding to 2 fb^{-1} data. A Gaussian function was fitted to the distribution in order to estimate the expected value for the zero point and sensitivity. The fit outputs are also shown in the picture.

[13] B. Aubert et al. Measurements of branching fractions, rate asymmetries, and angular distributions in the rare decays $B \to Kl^+l^-$ and $B \to K^*l^+l^-$. *Phys. Rev. D*, 73, 2006.

[14] A. Ishikawa et al. Measurement of Forward-Backward Asymmetry and Wilson Coefficients in $B \to K^*l^+l^-$. *Phys. Rev. Lett.*, 96, 2006.

[15] J. H. Lopes. Study of the rare decay $B_d \to K^*\mu^+\mu^-$ decay with the LHCb detector. (CERN-LHCb-2003-104).

[16] J. Dickens et al. Selection of the decay $B_d \to K^*\mu^+\mu^-$ at LHCb. (CERN-LHCb-2007-038).

[17] F. Marinho. *Quality Assurance of the VELO Modules and Analysis of the $B_d \to \bar{K}^*\mu^+\mu^-$ Rare Decay on LHCb*. PhD thesis, University of Glasgow, Glasgow, Scotland, 2008.

[18] I. Belyaev et al. *Gauss: LHCb Simulation Program*. LHCb, CERN, 1 / 1.4 edition.

[19] E. Parzen. On estimation of a probability density function and mode. *Ann. Math. Statist.*, 33:1065–1076, 1962.

[20] V. K. Murthy. Estimation of probability density. *Ann. Math. Statist.*, 36: 1027–1031, 1965.

[21] V. K. Murthy. Estimation of jumps, reliability and hazard rate. *Ann. Math. Statist.*, 36:1032–1040, 1965.

[22] F. Marinho. Studies on Sensitivity of the $B_s \to \mu^+\mu^-$ decay with the reoptimized LHCb detector. Master's thesis, IF, UFRJ, September 2005.

[23] B. Efron. Nonparametric estimates of standard error: The jackknife, the bootstrap and other methods. *Biometrika*, 68:589–599, 1981.

[24] N. Serra et al. Determination of the forward-backward asymmetry in the decay $B_d \to K^*\mu^+\mu^-$ with an unbinned counting analysis. (CERN-LHCb-09-003).